

## Identifying Overturns in CTD Profiles

PETER S. GALBRAITH

*Maurice Lamontagne Institute, Department of Fisheries and Oceans, Mont-Joli, Quebec, Canada*

DAN E. KELLEY

*Department of Oceanography, Dalhousie University, Halifax, Nova Scotia, Canada*

(Manuscript received 26 March 1995, in final form 10 October 1995)

### ABSTRACT

The authors propose a scheme to test whether inversions in CTD density profiles are caused by overturning motions (from which mixing rates may be inferred) or by measurement noise. Following a common practice, possible overturning regions are found by comparing the observed profile  $\rho(z)$  and an imaginary profile  $\hat{\rho}(z)$  constructed by reordering  $\rho(z)$  to make it gravitationally stable. The resulting "reordering regions" are subjected to two tests.

- The "Thorpe fluctuation" profile  $\rho'(z) = \rho(z) - \hat{\rho}(z)$  is examined for "runs" of adjacent positive or negative values. The probability density function (PDF) of the run length is compared with the corresponding PDF of random noise. This yields a threshold value for rms run length within individual reordering regions that must be exceeded for adequate resolution of overturns, taking into account both CTD characteristics and local hydrographic properties.

- Temperature and salinity covariations with respect to density are screened for systematic CTD errors such as those caused by time-response mismatches in temperature and conductivity sensors. Such errors may occur as the CTD passes through water-mass boundaries, for example, in interleaving regions. Resultant spurious inversions are avoided by the requirement of tight relationships between  $\rho$ ,  $T$ , and  $S$  within reordering regions.

The tests are calibrated with examples from coastal and deep-sea environments. The results suggest that a CTD may resolve overturns in coastal environments where mixing and stratification are large but that noise will prevent overturn detection for typical CTD resolution in the weakly mixed, weakly stratified, deep sea.

### 1. Introduction

Studies of ocean mixing are largely motivated by the need to parameterize the large-scale effects of mixing in models that are too coarse to resolve the finescale mixing processes. Traditional applications have often involved hydrodynamical modeling, but in recent years interest has arisen in biological studies as well. For example, it is thought that mixing shears may increase larval predator-prey interactions (Rothschild and Osborn 1988; MacKenzie and Leggett 1991) yielding a direct link between mixing properties and biology, for example Muelbert et al. (1994), beyond the well-known indirect links through nutrient fluxes to phytoplankton growth, etc. (Sverdrup 1955; McGowan and Hayward 1978; Cullen et al. 1983).

The length scale of motion for typical ocean mixing intensities is small enough (of the order of a few centimeters) to require specialized "microstructure" in-

struments such as shear probes. Since such devices are seldom found in standard hydrographic sampling packages, estimates of mixing are unavailable for the vast majority of oceanographic studies. Dillon (1982) suggested that this measurement gap could be spanned if certain properties of mixing could be inferred from readily obtained CTD measurements. Dillon pointed out that a key property is the scale of the overturning eddies. In stratified fluids, overturning eddies may be revealed by density "inversions"—regions with gravitationally unstable density gradients. The overturning scale is within the sampling range of CTD probes (of the order of a few meters), suggesting that CTD density inversions might yield a usable signature of otherwise unmeasured mixing. This raises the important possibility of enlarging the sparse mixing database by permitting mixing to be inferred in locations that have been sampled adequately with CTDs.

Several methods have been suggested to relate mixing rates to overturning properties, including the following:

- The rate of dissipation of turbulent kinetic energy  $\epsilon$  may be inferred from overturn thickness and buoyancy

---

*Corresponding author address:* Peter S. Galbraith, Maurice Lamontagne Institute, Department of Fisheries and Oceans, P.O. Box 1000, Mont-Joli, PQ G5H 3Z4, Canada.

frequency  $N$  by assuming that overturn thickness is equal to the ‘‘Ozmidov’’ length scale (Ozmidov 1965)

$$L_O = \left( \frac{\epsilon}{N^3} \right)^{1/2}. \quad (1)$$

(Here  $N$  is smoothed appropriately over the inversion; see Peters et al. 1995.) Good agreement has been reported between  $L_O$  and an estimate of overturn thickness defined by the so-called Thorpe scale  $L_T$  (Dillon 1982; Peters et al. 1988; Seim and Gregg 1994). [The Thorpe scale  $L_T$  is the rms vertical displacement required to reorder the observed profile  $\rho_i = \rho_i(z_i)$  into a gravitationally stable profile  $\hat{\rho}_i = \hat{\rho}_i(z_i)$  within the depth span enclosing the overturn (Thorpe 1977).]

• If overturning regions have TKE (turbulent kinetic energy) proportional to available potential energy and if the TKE is dissipated on a timescale proportional to the buoyancy period, then the dissipation rate should be given by

$$\epsilon = a \text{ APEF } N, \quad (2)$$

where  $a$  is an empirical coefficient measured to be 2.4–4.8 (Crawford 1986) and the APEF (available potential energy of the fluctuations) measures the perturbation potential energy of the overturn (Dillon 1984):

$$\text{APEF} = \frac{g}{n\rho_0} \sum_{i=1}^n z_i \rho'_i. \quad (3)$$

Here  $g$  is the acceleration of gravity,  $\rho_0$  is the average water density, and  $\rho'_i = \rho_i - \hat{\rho}_i$  is the ‘‘Thorpe fluctuation.’’ The sum in (3) may be applied to isolated overturns or to the whole water column.

• It may be that buoyancy flux, rather than  $\epsilon$ , is proportional to APEF  $N$ . Dillon and Park (1987) inferred this from the observation that APEF  $N$  was proportional to the buoyancy flux surrogate  $\kappa C_x N^2$  ( $\kappa$  being the molecular diffusivity and  $C_x$  the Cox number). This idea is difficult to test because buoyancy flux is difficult to measure directly (Moum 1990; Yamazaki and Osborn 1993).

The empirical value of  $a$  found by Crawford (1986) may be explained roughly by noting that APEF =  $N^2 L_T^2/2$  for an overturn in an initially linearly stratified density profile. Thus, substituting  $L_T \sim L_O$  into (1) yields  $\epsilon \sim 2 \text{ APEF } N$ . This calculation illustrates that these methods are empirical and semiquantitative. We also use assumptions that have not been fully tested in the literature; for example, the ratio of TKE to available potential energy should depend on the flux Richardson number, which may not be constant.

The question of which method is most accurate, or most useful in practice, has yet to be answered. Indeed, we will leave this question open and concentrate instead on a more basic question: how to identify overturning regions in CTD profiles given instrumental noise and other constraints. Note that overturn identi-

fication is important in each of the methods listed above. Clearly, overturn thickness is needed in the first method since  $\epsilon$  depends on the square of the thickness; in the other methods, identifying individual overturns allows calculation of mixing properties as a function of depth and the exclusion of the APEF of spurious overturns.

In this paper we outline an analysis scheme designed to flag spurious density inversions formed by various types of instrument noise. This scheme is designed to reject inversions caused by noise or systematic errors. The latter include the problem of salinity spiking associated with the mismatch in time response of temperature and conductivity sensors, discussed at length by many authors (e.g., Perkin and Lewis 1982; Horne and Toole 1980; Topham and Perkin 1988), and the more recently recognized problem, which occurs on longer timescales, arising from the thermal inertia of the conductivity cell itself (Lueck 1990; Lueck and Picklo 1990; Morison et al. 1994). Our proposal does not replace the need for careful data acquisition practices and for postprocessing to minimize the effects of the aforementioned problems.

In sections 2 and 3 we outline the components of the scheme, and in sections 4 and 5 we illustrate with oceanic examples spanning a representative range of mixing conditions and stratification levels. In sections 6 and 7 we discuss more generally the feasibility of using finescale properties to infer microscale mixing rates.

## 2. Resolution limits on overturn detection

### a. Inversions and reordering regions

Buoyancy forces cause heavy fluids to sink through lighter ones. The result is that stratified fluids at rest have  $\partial\rho/\partial z < 0$ . Thus, regions with reversed gradients—so-called density inversions—are thought to signal overturning motions.<sup>1</sup>

The idealized case of a cylindrical overturning eddy in an initially linear density profile yields a Z-shaped  $\rho(z)$  segment. This simple picture is seldom seen in practice, partly because turbulent overturning motions contain motions at smaller scales (Thorpe 1984, 1985). Although scaling laws have been proposed for early stages of Kelvin–Helmholtz mixing (e.g., Caulfield and Peltier 1994), many details remain to be worked out. Nevertheless, it is clear that mixing motions have length scales considerably smaller than the overturn scale so that  $\rho(z)$  will have smaller scale variations superimposed on the idealized Z shape. Unfortunately, there is another factor. Instrument noise may yield pat-

<sup>1</sup> Strictly speaking, gravitationally unstable gradients will not lead to convective overturning unless the Rayleigh number exceeds a critical value  $Ra_c \sim 10^3$ . But  $Ra = g\Delta\rho H^3/(\rho\nu\kappa)$  exceeds  $10^3$  at the limit of CTD resolution ( $\Delta\rho \sim 0.001 \text{ kg m}^{-3}$  and  $H \sim 0.02 \text{ m}$ ), so all detectable inversions should be subject to overturning motion.

terns of similar scales, making it difficult to infer overturns from density profiles.

In typical density profiles, the sign of  $d\rho/dz$  changes repeatedly (see Fig. 1). The resultant inversions have scales ranging from a presumed eddy scale, inferred from the general shape of the profile, down to the vertical resolution of the instrument. Density variations at the resolution scale cannot reasonably be ascribed to mixing motions; such unresolvable features fall into a class that we denote as noise.

Although density inversions suggest the existence of overturns, they are poor measures of their depth span. Dillon (1984) suggested that a better measure was the scale of "complete overturns." Corresponding to a given inversion, this is the minimal depth interval spanning all the density data that are shuffled during the reordering process. For example, in Fig. 1 the reordering procedure identifies two regions of possible overturning (shown in dashed boxes). The division into regions can be illustrated by examining the deeper region, spanning  $A$  to  $B$ . The point  $z = A$  is defined as the maximal depth such that all the overlying fluid is of lesser density than all the underlying fluid. Similarly, all the fluid below  $z = B$  is denser than the maximum density in the interval  $A$  to  $B$ . At the risk of proliferating notation, we refer to such regions as "reordering regions" instead of complete overturns to emphasize the computational aspect of the definition and avoid the implication that the reordering method actually identifies overturning, as opposed to noise.

#### b. Resolution of overturn thickness

Instrument resolution imposes basic constraints on overturn detection. To begin with, the Nyquist sampling theorem means that overturns thinner than twice the vertical resolution  $\delta z$  cannot be measured. More robust determinations can be made if more samples are available, leading to several rules of thumb for the minimum number of samples per resolved wavelength. Koch et al. (1983) suggest that five samples are sufficient, while Levitus (1982) suggests that seven to eight are needed. An optimistic rule of thumb, then, is that the constraint of vertical resolution allows the detection of overturns no thinner than

$$L_z \approx 5\delta z. \quad (4)$$

Another limit results from the need to measure the density differences associated with overturns. To distinguish between the minima and maxima of a signal, the density resolution  $\delta\rho$  must be less than the signal amplitude. The use of a safety margin suggests that an instrument with density resolution  $\delta\rho$  can measure overturns no thinner than

$$L_p \approx 2 \left| \frac{\delta\rho}{\partial\rho/\partial z} \right|, \quad (5)$$

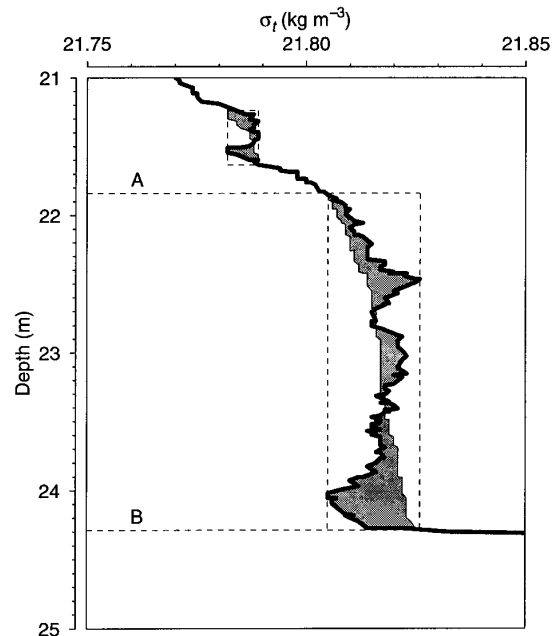


FIG. 1. CTD profile in the St. Lawrence estuary (SLE) showing measured  $\rho(z)$  (thick line, sigma density units), reordered profile  $\hat{\rho}(z)$  (thin line), and Thorpe fluctuation  $\rho'(z) = \rho(z) - \hat{\rho}(z)$  (shaded area). Depths  $A$  and  $B$  span a "complete overturn" [Dillon's (1984) notation] or reordering region (our notation). A second reordering region is delineated by the smaller dashed box above.

where  $\partial\rho/\partial z$  is smoothed over a scale exceeding the overturn scale. In terms of the appropriately smoothed buoyancy frequency, this is

$$L_p \approx 2 \frac{g}{N^2} \frac{\delta\rho}{\rho_0}, \quad (6)$$

where  $\rho_0$  is a representative mean density. For example, a CTD capable of resolving density differences of  $\delta\rho \sim 10^{-3} \text{ kg m}^{-3}$  cannot detect overturns thinner than 0.02 m if  $N \sim 0.03 \text{ s}^{-1}$  (e.g., in an estuarine or coastal environment) or 2 m if  $N \sim 0.003 \text{ s}^{-1}$  (e.g., in a deep-sea environment). CTD vertical resolution less than  $\delta z \sim 0.1$  m implies that overturns smaller than approximately 0.5 m cannot be resolved [from (4)]. Thus, we expect overturn detection to be limited equally by density and by vertical resolution in weakly stratified regimes but mostly by vertical resolution in highly stratified regimes.

#### c. Resolution of dissipation rate

The possibility of detecting overturns in an area of interest can be grossly evaluated if the mixing rate is approximately known. Using (1) and assuming that the overturn thickness equals Ozmidov scale, the minimal detectable dissipation rate can be calculated as

$$\epsilon_z \approx 25(\delta z)^2 N^3, \quad (7)$$

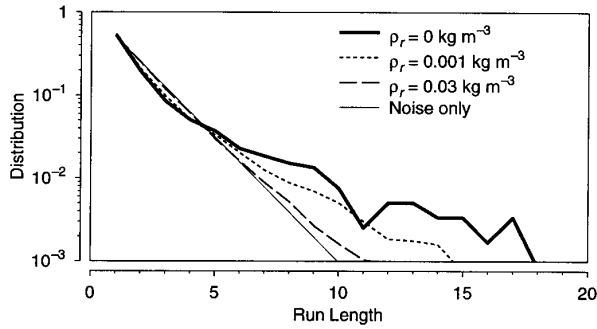


FIG. 2. Probability density function of the Thorpe fluctuation run lengths for an observed profile (thick line), and with the addition of increasing amounts of random, uncorrelated noise  $\rho_r$  (dashed lines). Also shown is the PDF of noise added to a linear density gradient (thin solid line).

given the vertical resolution  $\delta z$  and (4). Density resolution sets the additional limit

$$\epsilon_\rho \approx 4 \frac{g^2}{N} \left( \frac{\delta \rho}{\rho_0} \right)^2 \quad (8)$$

from (6). Only signals exceeding both (7) and (8) can be resolved. These criteria rely on the assumption that  $L_T \sim L_O$  and so are meant only to be used as rough estimates.

### 3. Practical overturn detection

#### a. Resolution versus practical detection

The resolution limits on overturn thickness (section 2b) and dissipation rate (section 2c) provide crude lower bounds on measurable signals. However, it remains to be seen whether resolvable mixing signatures will be detectable *in practice*, given CTD sampling errors (e.g., temperature and conductivity mismatch and thermal lag) and the complicated nature of overturning. Consider the rule of thumb that five to eight samples being required per wavelength. Might five samples be sufficient, given that the Nyquist theorem requires only two? Or might 10 be too few to yield statistical robustness? Since more data yield more reliable statistical results, caution might suggest discarding all short re-ordering regions. But the cost of caution may be to miss real mixing events. On the other hand, judging questionable regions to be overturns will yield mixing estimates that merely reflect noise. A balance must be attained.

Ideally, the predictive power of the signatures would be gauged using direct measurements of overturning, but such measurements—for example, two-dimensional snapshots—are not generally available. In the laboratory, shadowgraph visualization allows fairly direct observation of overturning, but such studies are seldom accompanied by fine structure and microstructure mixing measurements. In the ocean, there have

been many useful profiling and towed-chain studies (Thorpe et al. 1977; Washburn 1987; Hebert et al. 1992), some of which also employed microstructure sampling, but direct Lagrangian observation of overturning has only rarely been attempted, a notable exception being the dye injection measurements of Woods (1968).

Lacking ground-truth measurements, we will simply postulate signatures based on expected overturn properties and instrument difficulties. A similar approach of postulating signatures without ground-truth testing has been used to infer mixing properties in towed-chain measurements (e.g., Mack 1989; Mack and Schoeberlein 1993). Our study is similar in spirit. The desire for results—in this case, to determine whether archived CTD data might provide information on mixing rates—outweighs the worry of being unable to corroborate our inferences with measurements.

In the next two sections, a suggested noise-rejection scheme is presented. The first part is a refinement of the depth and density resolution limits, using the “run-length” statistical property. The second seeks to reject density inversions caused by spurious  $T-S$  covariation, such as those resulting from mismatches in time constants of temperature and conductivity sensors or from the thermal lag of the conductivity cell.

#### b. Run-length test

Spurious density inversions can arise if noise is added to a smoothly stratified profile. The run-length statistical measure may be useful in detecting such inversions.

The standard statistical property known as run length is defined as follows. The points in a time series are examined sequentially and adjacent values of one sign are grouped into sets called “runs.” For a random, uncorrelated time series with equal numbers of positive and negative values, the probability density function (PDF) of run length is

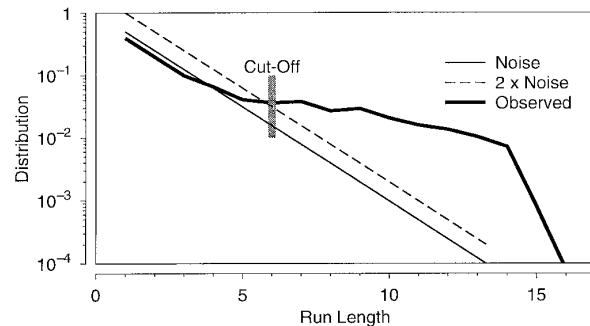


FIG. 3. Definition of run-length criterion showing run-length PDF (thick line); the PDF of noise added to linear density gradient (thin line) and double the latter (dashed line). The cutoff run length is defined at first crossover point between the observed PDF and double the noise PDF.

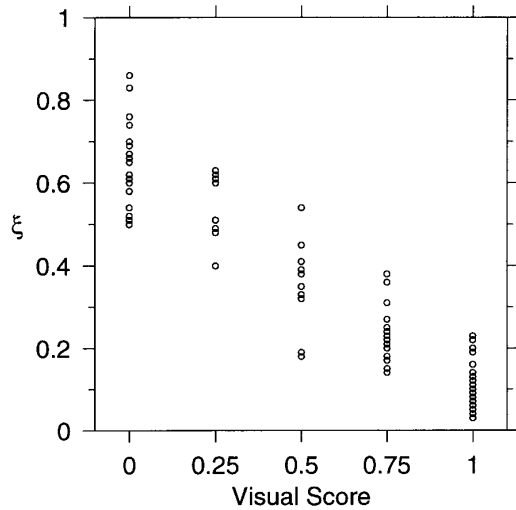


FIG. 4. Comparison of water-mass criterion  $\xi$  and visual scoring of "tightness" of  $T$ - $S$  diagrams.

$$P(n) = 2^{-n}, \tag{9}$$

where  $P(n)$  is the probability of a run of length  $n$  (e.g., Larson and Marx 1986). Consider a linear gravitationally stable density profile to which random density noise is added. The run-length PDF of the Thorpe fluctuation series is expected to obey (9) if the noise amplitude is sufficient to create inversions. In contrast, for real overturns, the Thorpe fluctuations have a long positive run in the top half of the overturn and a long negative run in the bottom half. This is demonstrated in Fig. 2, which shows the results of a Monte Carlo experiment in which random noise  $\rho_r$  has been added to an observed profile (from the EUBEX dataset, discussed below). The observed PDF deviates from the noise PDF, with more longer runs (and therefore fewer short runs, since the integrated PDF is the same for both cases), but the addition of random noise reshapes the PDF into (9). This example demonstrates that while (9) is theoretically expected for a *linear* (reordered) density profile, it is also a valid approximation of the PDF expected for a typical *nonlinear* density profile. Thus, the result appears to be robust.

This suggests a test for noise-induced inversions, based on the difference between the observed run-length PDF and (9). With no accepted statistical model of overturning, we have little theoretical guidance for measuring the difference between the two PDFs. We suggest an ad hoc scheme, in which the minimal acceptable run length is defined as the shortest run length at which the observed occurrence rate is double that predicted by (9). Figure 3 illustrates the criterion. Our doubling requirement is wholly empirical and was guided by visual inspection of dozens of reordering ranges.

As a diagnostic of the typical run length within a reordering region, we chose the rms value. Statistically,

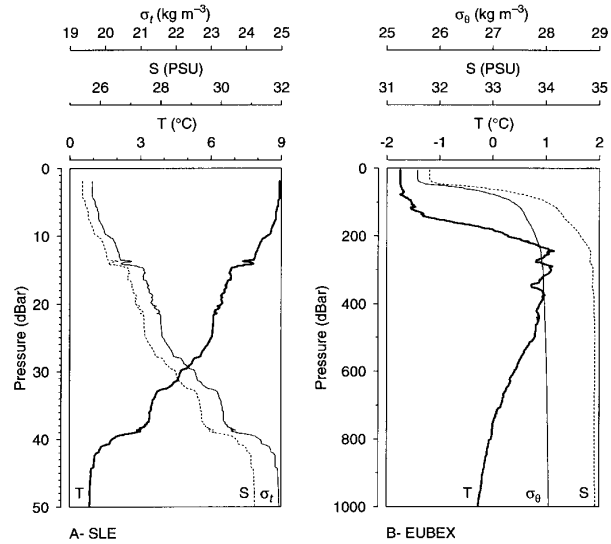


FIG. 5. Sample profiles used in analysis. (a) CTD profile at the head of the Laurentian channel in the SLE. (b) Profile 206 of the EUBEX dataset acquired near Svalbard.

this corresponds to forming a mean value of run length, with individual runs being weighted by the thickness of water they represent.

The test procedure then, is to discard any reordering regions in their entirety that have rms run length less than the cutoff run length. The cutoff is calculated from a sample set considered representative of the physical regime of interest, for example, the whole CTD cast or all casts in the geographical region.

*c. Water-mass test*

Density inversions that pass the run-length test are unlikely to result from random CTD noise, but they may result from systematic noise, such as that resulting from mismatches in time response of temperature and conductivity probes or from the thermal inertia of conductivity cells. The problem is worst when the CTD passes through regions in which  $T$  and  $C$  vary rapidly

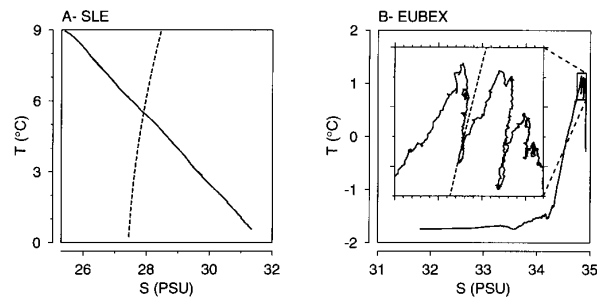


FIG. 6. Temperature-salinity diagrams corresponding to the profiles of Fig. 5. The dashed lines are selected isopycnals.

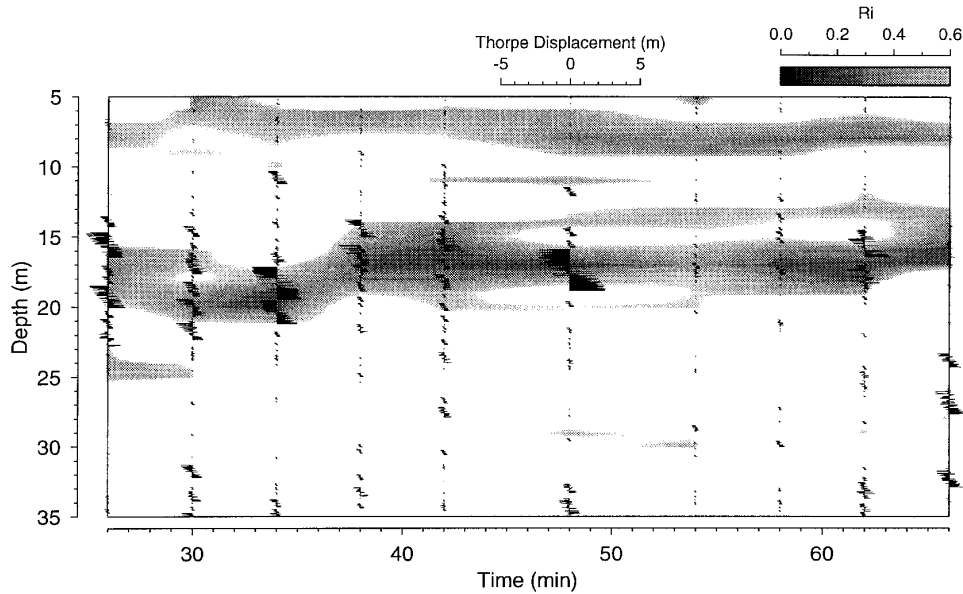


FIG. 7. Richardson number (gray scale) and Thorpe displacements (filled profiles) for 10 consecutive SLE CTD profiles taken over 40 min, starting with the profile in Figs. 5 and 6. Only reordering regions with more than four points are shown.

(whether or not salinity varies at all). This includes regions of density-compensated lateral intrusions, as may be formed by double diffusion.

On a  $T-S$  diagram, spurious inversions may appear as loops at the base of the near-isopycnal  $T-S$  changes representing the lateral intrusions (see examples later) even after all precautions have been taken during data acquisition and careful postprocessing has been done. It is a common practice to inspect  $T-S$  diagrams visually and to smooth the data over a scale chosen to eliminate the loops; automated methods might examine the scale dependence of the  $T-S$  phase relationship. Smoothing profiles is akin to a possible conservative approach to this problem in our context—namely, to discard reordering regions near intrusions. Unfortunately, the cost of being conservative could be to miss overturning motions in precisely the regions of most interest. This cost can be illustrated with two schemes that have been used to process CTD data. First, it has been suggested that  $T$  and  $C$  signals should be postpro-

cessed with filters whose coefficients have the effect of minimizing the APEF of density inversions. Clearly, this would adversely affect the possibility of using our technique. An even more limiting processing technique would be to discard all density inversions, completely erasing Thorpe-based mixing signals.

A reasonable scheme may be to discard only those reordering regions in which a large variation in water-mass characteristics is observed. If a region of smooth  $T-S$  covariation is subjected to an overturn, the heavy water at the top of the overturning patch will lie on the same  $T-S$  line as the light water at the bottom of the patch, independent of the vertical shuffling. Thus, the smoothness of the  $T-S$  diagram is unaffected by overturning. However, time-constant mismatches will lead to deviations from the original  $T-S$  curve. One method for rejecting these spurious inversions is to perform the reordering procedure on both  $\rho$  and  $T$ , rejecting reordering regions that are significantly different according to the two methods (Peters et al. 1995). This approach requires matching reordering regions from the two techniques, which may be difficult when the  $T$  and  $\rho$  reordering regions lack a one-to-one mapping (e.g., a given reordering region in one variable might span several reordering regions in the other).

We seek to measure this  $T-S$  deviation in a way that is independent of the units of  $S$  and  $T$ . We also seek to acknowledge that  $T$  and  $S$  may contribute unequally to density.

Our scheme examines each reordering region individually. Least squares curve fits are done for the points within the individual reordering regions. We use the

TABLE 1. Resolution limits for SLE and EUBEX test data.

	SLE	EUBEX
Vertical resolution $\delta_z$ (m)	0.02	0.25
Density resolution $\delta\rho$ ( $\text{kg m}^{-3}$ )	0.001	0.001
Buoyancy frequency $N$ ( $\text{s}^{-1}$ )	0.03	0.003
Overturn resolution $L_z$ (m)	0.1	1.25
Overturn resolution $L_\rho$ (m)	0.02	2
Dissipation resolution $\epsilon_z$ ( $\text{m}^2 \text{s}^{-3}$ )	$3 \times 10^{-7}$	$4 \times 10^{-8}$
Dissipation resolution $\epsilon_\rho$ ( $\text{m}^2 \text{s}^{-3}$ )	$1 \times 10^{-8}$	$1 \times 10^{-7}$

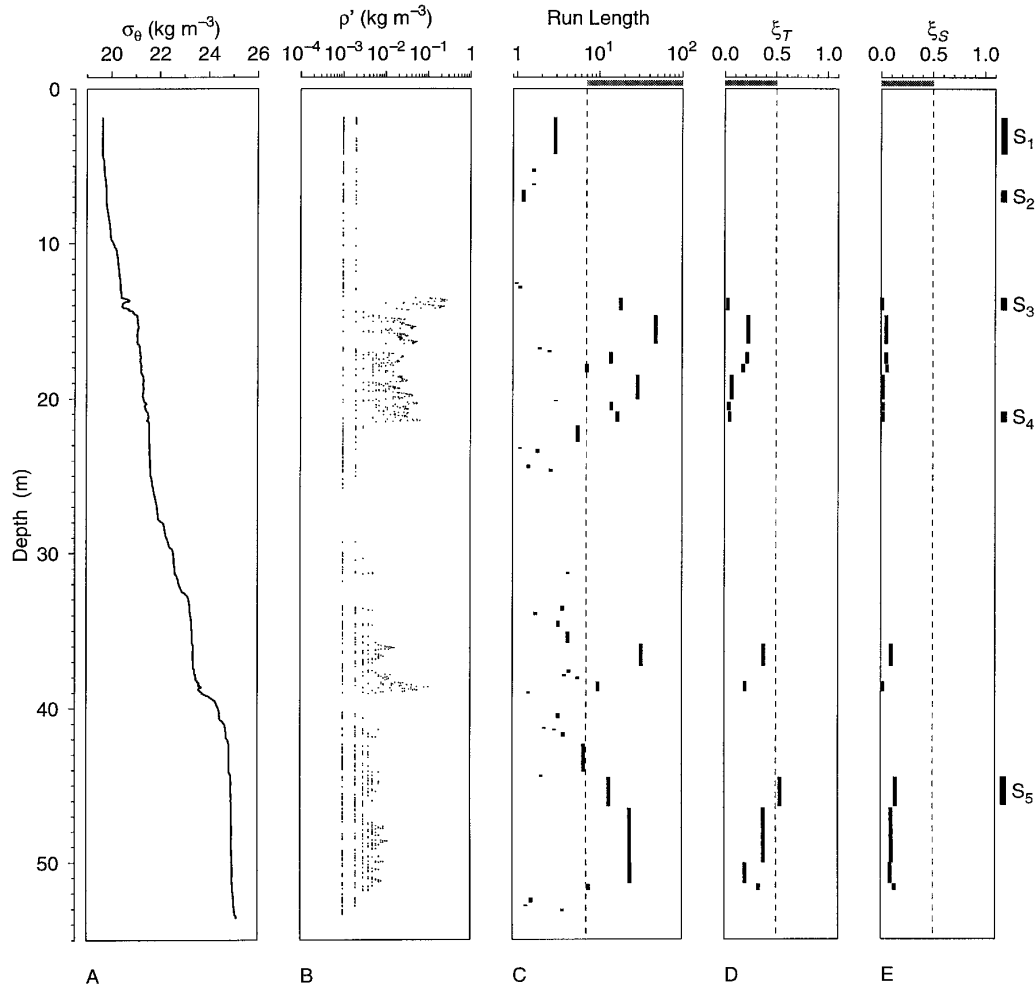


FIG. 8. Reordering regions for SLE case showing (a) density profile; (b) absolute value of the Thorpe fluctuation; (c) rms run length indicated (by vertical lines) for reordering regions with more than four points, eliminating only inversions that fail our criteria; (d)  $\xi_T$ ; and (e)  $\xi_S$ . Only reordering regions that pass the run-length test are shown in (d) and (e). Cases with run length of at least 7 and  $(\xi_T, \xi_S)$  less than 0.5 [shaded regions of panels (c)–(e)] are suggested indicators of overturning. Regions labeled  $S_1$ – $S_5$  are discussed in detail in the text.

simplest models of smooth  $T$ – $S$  covariation, namely,  $\rho_S = a_S + b_S S$  and  $\rho_T = a_T + b_T T$ . The deviations between the observations and these lines are measured by computing the rms values of  $\rho - \rho_S$  and  $\rho - \rho_T$ . These are made nondimensional by dividing by the rms Thorpe fluctuation  $[N^{-1} \sum_{i=1}^N (\rho - \hat{\rho})^2]^{1/2}$ . Roughly speaking, the division by rms Thorpe fluctuation scales the  $T$  and  $S$  deviations to the density amplitude of the suspected overturn. The resultant ratios, denoted  $\xi_S$  and  $\xi_T$ , respectively, are positive-definite quantities that approach 0 for tight  $T$ – $S$  relationships and that exceed 1 for rather loose relationships. When  $T$  or  $S$  contributes overwhelmingly to density variation, the larger contributor tends to have low values of  $\xi$ , so our test is applied to  $\xi = \max(\xi_S, \xi_T)$ .

To determine a critical value of  $\xi$ , we visually inspected the reordering regions within the SLE dataset

(described below) that passed the run-length test. Individual reordering regions were scored on a qualitative scale from 0 to 1, according to the tightness of the  $T$ – $S$  relationship. (We employed visual inspection, rather than some numerical measure, so we could easily apply penalties for large rms deviation or large individual deviation.) We assigned scores below 0.5 to reordering regions that would be discarded by the usual visual method of rejecting regions with loops in the  $T$ – $S$  diagram. The results of this scoring procedure were compared with measured values of  $\xi$  as a crude calibration of our test (Fig. 4). The correlation coefficient between the visual score and  $\xi$  is  $R^2 = 0.88$ . Based on the tight relationship between  $\xi$  and visual score, we assign a critical value  $\xi_c = 0.5$ . Only reordering regions with  $\xi < \xi_c$  are judged to have  $T$ – $S$  relationships sufficiently tight to be regarded as signatures of overturning mo-

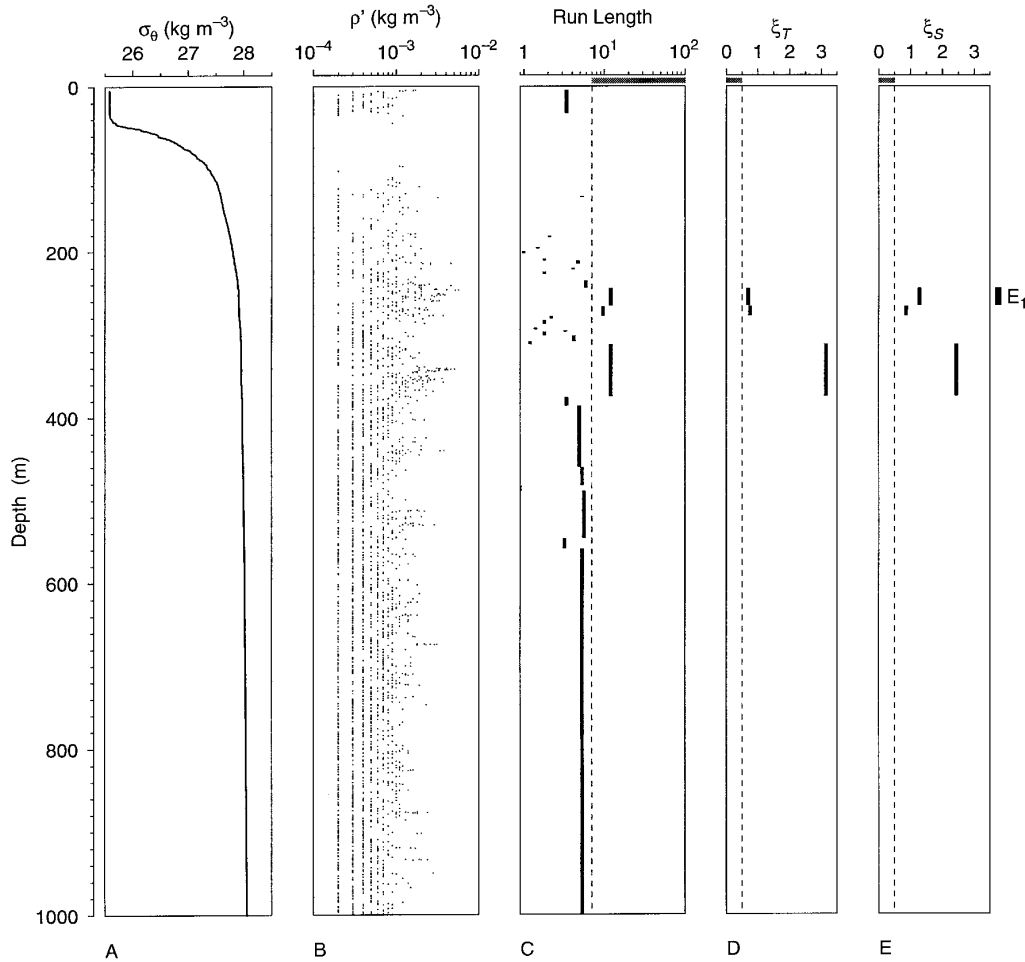


FIG. 9. As Fig. 8 for the EUBEX case. A few reordering regions pass the run-length test

tion. A physical interpretation of this value is that it requires the density variation about a linear base state in  $T-S$  space to be less than half the typical convective density anomaly in the suspected overturning region.

**4. Test data**

*a. Oceanographic setting*

Two CTD profiles are used for illustration (Fig. 5). The ‘‘SLE’’ measurements were made in the St. Lawrence estuary, Canada. The ‘‘EUBEX’’ measurements were made near Svalbard ( $84^{\circ}\text{N}$ ,  $1^{\circ}\text{E}$ ), where warm salty Atlantic water interacts with cold fresh Arctic water. The datasets represent opposite ends of the mixing spectrum, SLE being a highly stratified and vigorously mixed coastal regime and EUBEX being a more weakly stratified and less vigorously mixed deep-sea regime. An additional difference is that the EUBEX measurements are in a region of prominent interleaving (Lewis and Perkin

1983; Perkin and Lewis 1984). This is indicated by large ( $\sim 50$  m)  $T$  variations in Fig. 5; the  $T-S$  diagram of Fig. 6 makes the case more clearly, illustrating that the  $T$  variations are largely compensated in density terms by  $S$  variations.

We use a single profile for the EUBEX case, taken using a Guildline Mark IV CTD. The details of calibration and data acquisition are described in Lewis and Perkin (1983). In the SLE case, more profiles are available since the experiment was designed specifically to investigate mixing. High-resolution ( $\delta z = 0.02$  m) CTD profiles were taken at 4-min intervals using a Guildline Mark IV CTD lowered at a rate of  $0.4$  m  $\text{s}^{-1}$  in very calm seas. The drop rate was fairly constant, and depth reversals never occurred. The sensors were positioned at the leading end of the pressure casing to keep them out of its turbulent wake. Only downcasts were used, sampled at 25 Hz. ADCP shears were measured using a R&D Instruments 1200-KHz ADCP. The Richardson number  $\text{Ri}(z, t)$  was calculated using buoyancy frequency computed from reordered density

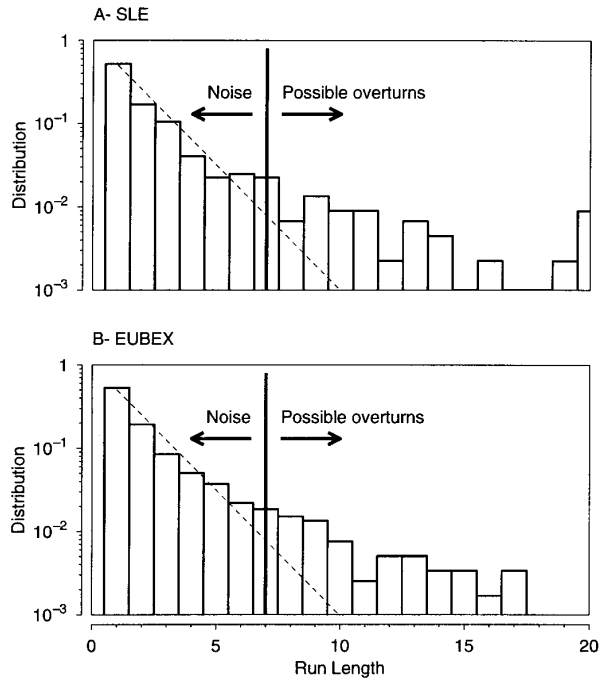


FIG. 10. Run-length histograms of Thorpe fluctuations in (a) SLE and (b) EUBEX cases. The solid line is the observed histogram, while the dashed line is the PDF  $P = 2^{-n}$  of a random series. The threshold run length between unresolved noise and possible overturns is seven in each case.

profiles, smoothed with a 3-m triangular filter to match the wavenumber response of velocity measured with the R&D Instruments ADCP. The resultant depth resolution of  $Ri$  is of the order of several meters.

The SLE  $Ri(z, t)$  field has regions of low  $Ri$  (Fig. 7), indicative of the potential for Kelvin–Helmholtz overturning and mixing. These regions are seen near the top of the water column and between 15- and 20-m depth. There is a reasonable correspondence between areas of low Richardson number and regions of large density inversions, as indicated by Thorpe displacement. This preliminary comparison suggests that the CTD is, in fact, responding to mixing signals instead of noise. We note, however, the presence of many small inversion regions generally removed from low- $Ri$  regions. A natural question is whether these inversions are caused by noise.

#### b. Resolution limits

Table 1 shows SLE and EUBEX resolution limits, following the analysis of sections 2b and 2c. The SLE data can only resolve overturns thicker than 0.1 m and dissipation rates greater than approximately  $10^{-7} \text{ m}^2 \text{ s}^{-3}$ , with depth resolution being the limiting factor by an order of magnitude. Resolution in the EUBEX case is limited almost equally by depth and density resolution. EUBEX resolution of  $\epsilon$  is similar to that in

SLE, but the resolution of overturn thickness is an order of magnitude poorer.

We must emphasize that the resolvable mixing rates are orders of magnitude larger than the noise floor of conventional microstructure instrumentation  $\epsilon \sim 10^{-10} \text{ m}^2 \text{ s}^{-3}$ . This illustrates the important point that inference of mixing rates from finescale observations cannot be expected to replace microstructure instrumentation in general; it is unlikely to be useful in regions of weak mixing. The hope, however, is that the technique applied in vigorously mixed regions that have been sampled by CTD but not microstructure probes. The reasonable depth-time correspondence of Richardson number and large Thorpe displacement illustrated in Fig. 7 provides a case in point.

Given these rough estimates of resolution of our technique, might one expect to detect mixing in our test cases? For EUBEX, the prospects are poor since the resolution limit is of the same order of magnitude as the average value  $\epsilon \sim 10^{-7} \text{ m}^2 \text{ s}^{-3}$  measured by Padman and Dillon (1991). However, since the observed dissipation rates sometimes exceeded the mean by an order of magnitude, it might be possible to resolve large mixing events, implying that further consideration is warranted. For SLE the method appears to be more promising. No dissipation measurements are available for SLE, but assuming tidal friction to be the source, we estimate  $\epsilon \sim C_d U^3 / H \sim 10^{-6} \text{ m}^2 \text{ s}^{-3}$ , (using drag coefficient  $C_d \sim 10^{-3}$ , tidal velocity  $\sim 0.5 \text{ m s}^{-1}$ , and water depth  $H \sim 100 \text{ m}$ ). Thus, the expected signal is an order of magnitude greater than the resolution limit, suggesting that the reordering method should give useful results in the SLE case.

## 5. Application of criteria to test data

### a. Overview

Diagnostic diagrams for SLE and EUBEX are shown in Figs. 8 and 9, respectively.

Several SLE inversions are easily visible. A prominent example is associated with the reordering region marked  $S_3$ , at 14-m depth. Casual inspection reveals that the density anomaly is of order  $0.1\text{--}1 \text{ kg m}^{-3}$ , clearly above the instrumental resolution of about  $0.001 \text{ kg m}^{-3}$ . Furthermore, the  $O(1)$ -m thickness greatly exceeds the CTD depth-resolution limit of 0.02 m. Thus, the inversion is well above the limit of resolution. The absence of density variations of similar magnitude in the rest of the profile suggests that the inversion is not caused by noise. Furthermore, examination of Figs. 5 and 6 shows that this inversion does not deviate from the overall (linear)  $T$ – $S$  relationship, eliminating the possibility that it results from temperature and conductivity sensor time-constant mismatches. These considerations strongly suggest that the reordering region  $S_3$  signals actual overturning motion.

Other reordering regions in the SLE case are harder to detect visually. For example, Fig. 8b shows apparent

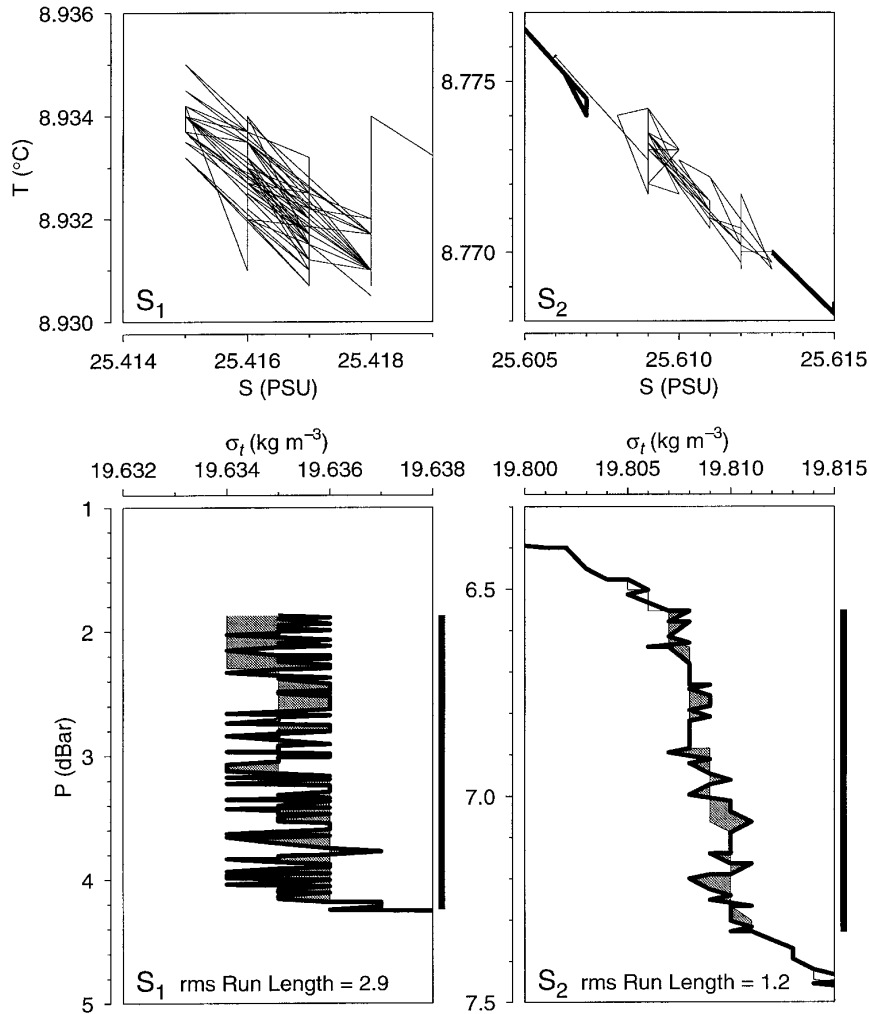


FIG. 11. Examples of reordering regions that fail the run-length test. Left: reordering region  $S_1$  of Fig. 8. Right: reordering region  $S_2$ . Lines and shading on bottom panels are as in Fig. 1 and vertical lines to the right indicate depth spans of reordering regions.

overturning in a region extending approximately 10 m below the reordering regions  $S_3$  and a thinner reordering region at about 39 m.

There is little visual indication of inversions in the EUBEX density profile in Fig. 9a, although the other panels of the figure indicate many density inversions. Some of the reordering regions are much too large to represent individual overturns. For example, consider the reordering region covering a 400-m span near the bottom of the profile. According to (1), a cylindrical overturn this thick embedded in a region with  $N \sim 0.003 \text{ s}^{-1}$  should have dissipation rate  $\epsilon \sim 4 \times 10^{-3} \text{ m}^2 \text{ s}^{-3}$ . This cannot be reconciled with observed values, which are three to four orders of magnitude smaller (Padman and Dillon 1991), implying that the long reordering regions must result from noise and should be discarded. Still, might the less dramatic reordering regions result from actual overturning? The next sub-

sections illustrate how our tests may help to answer this question.

*b. Run-length test*

The Thorpe fluctuation run-length PDF for the sample profiles of Fig. 5 is shown in Fig. 10. The dashed lines indicate the PDF of random noise calculated with (9). For short runs, the observed PDF is very similar to the noise PDF. These short runs are therefore indistinguishable from noise. In contrast, long runs are much more frequent than would be expected for noise-induced inversions. In both SLE and EUBEX, runs longer than about 7 occur twice as often as would be expected if the inversions had been caused by random noise added to an inversion-free profile. Therefore, we consider runs shorter than 7 to be indistinguishable from noise and regard the reordering regions with rms run length smaller than 7 as being spurious.

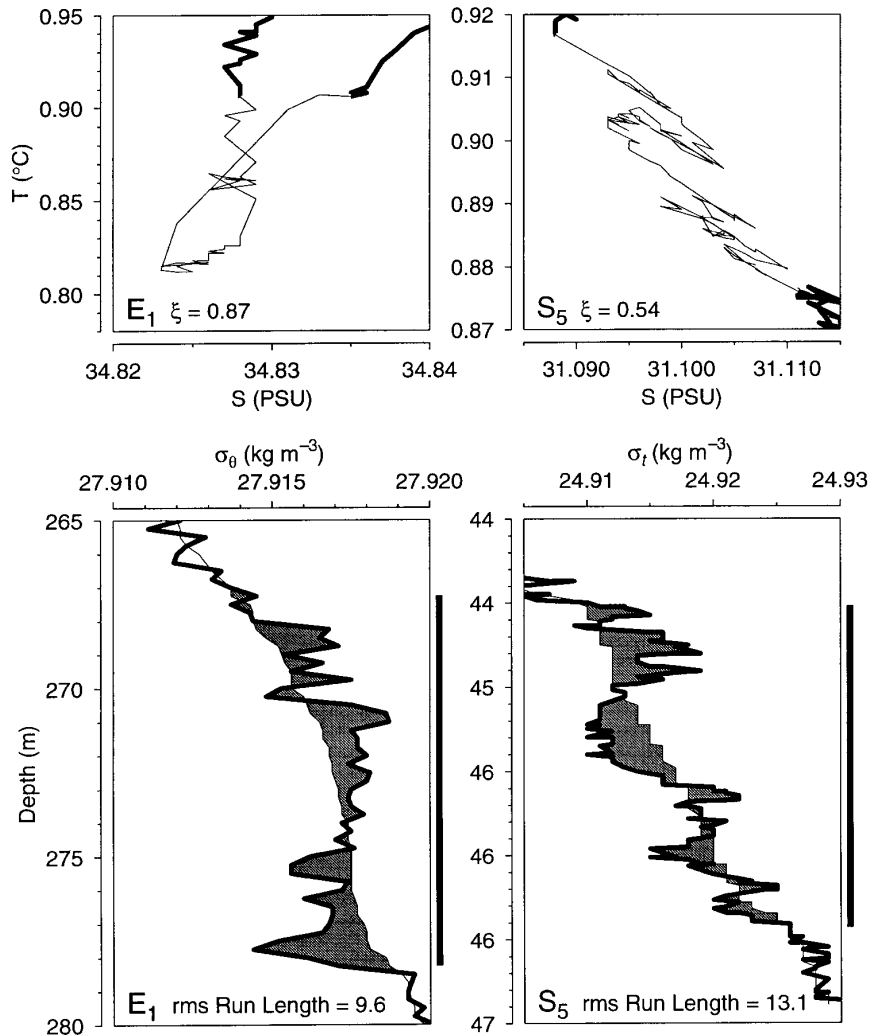


FIG. 12. Examples of reordering regions that pass the run-length test but fail the  $T$ - $S$  test. Values of  $\xi$  are indicated on top panels. Note prominent looping in  $E_1$  (compare with Fig. 6).

The two SLE reordering regions marked  $S_1$  and  $S_2$  on Fig. 8 are illustrated in greater detail in Fig. 11. The rms run lengths are respectively 2.9 and 1.2, substantially lower than the cutoff value. Both reordering regions  $S_1$  and  $S_2$  are therefore rejected in their entirety. Visual inspection of the Fig. 11 density profiles suggests that these reordering regions might result from random density perturbations added to weakly stratified profiles, with the Thorpe fluctuations being alternatively positive and negative. Furthermore, the Thorpe fluctuations  $\rho'$  in  $S_1$  are comparable to the CTD resolution ( $\delta\rho = 0.001 \text{ kg m}^{-3}$ ) so that  $S_1$  fails the density resolution requirement of (6), given the low value of  $N$ . [We have found that reordering regions near the  $(\delta z, \delta\rho)$  resolution limits usually fail the run length test, although it is prudent to first reject any reordering regions having rms Thorpe fluctuations near  $\delta\rho$  or Thorpe scales near  $\delta z$ .]

It is worth noting that the 400-m-thick reordering region near the bottom of the EUBEX profile has an rms run length that fails our test. The entire reordering region is therefore rejected. Unfortunately, overturning is not resolvable in this depth span because noise in the density measurements creates an apparent instability that requires the entire 400-m span to be used in order to sort it to monotonically increasing density. Another diagnostic test that also flags this reordering region as being questionable is the ratio of Thorpe scale to the depth span of the reordering region. For a Z-shaped inversion, this ratio is of order unity. For this case, however, the ratio is about 0.02.

### c. Water-mass test

Two reordering regions that pass the run-length test but fail the water-mass test are shown in Fig. 12. Al-

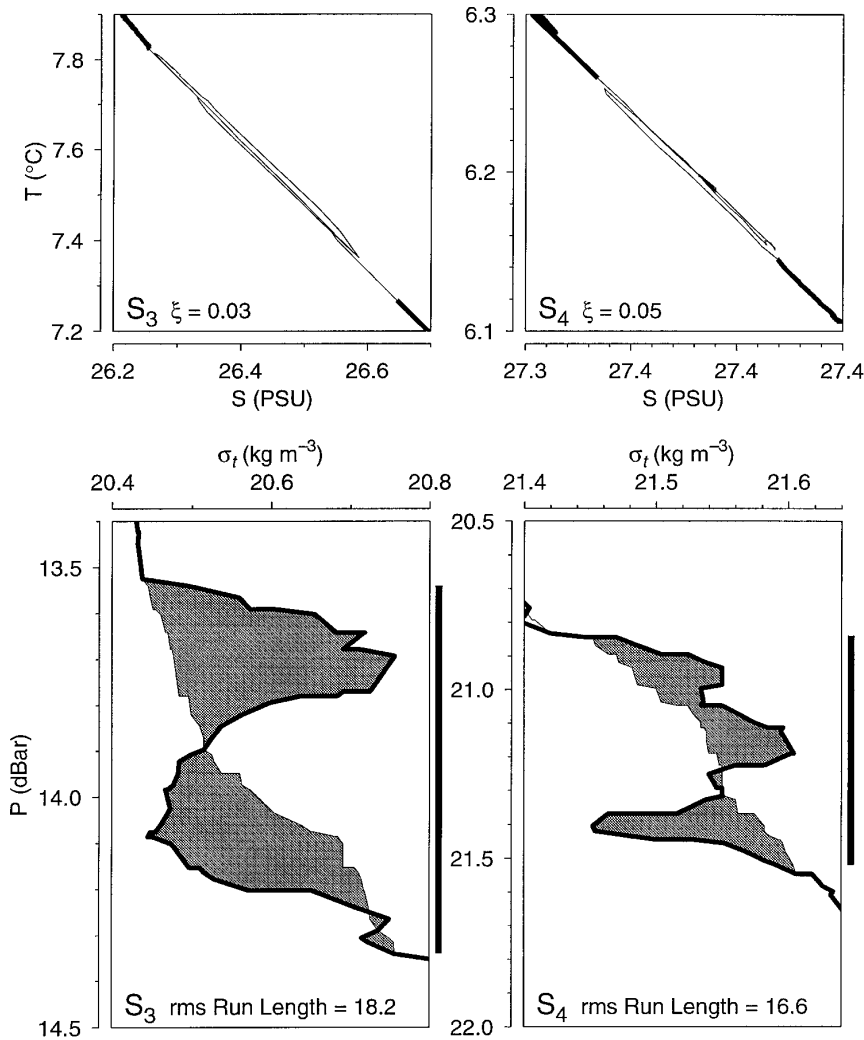


FIG. 13. Two reordering regions that pass both the run-length and water-mass tests.

though no visible looping is seen in S<sub>5</sub>, the jagged T–S offset appears to indicate that the reordering region contains more than one water mass. Perhaps this is caused by sensor mismatch and could be sufficiently reduced by some data postprocessing to pass our water-mass test. This is a reminder that our criteria are designed to reject inversions associated with sampling error and not to fix these errors.

The E<sub>1</sub> case is a thick reordering region, spanning 20 m vertically, located at the core of an interleaving water mass (see Fig. 5). The T–S diagram has a prominent loop at this location, a classic signature of spurious density anomalies resulting from temperature–conductivity sensor mismatch. Such loops translate into a smoothly varying top-heavy signature on density profiles that might appear to be a cleanly sampled overturning region. Case E<sub>1</sub> is thus a good illustration of one intention of the water-mass test—to reject spurious

overturns caused by temperature–conductivity sensor mismatch.

*d. Examples of acceptable reordering regions*

Two examples illustrate the T–S and ρ(z) characteristics of reordering regions that pass the proposed tests (Fig. 13). Each easily meets the resolution requirements, being about 1 m thick, with Thorpe fluctuation of approximately 0.1 kg m<sup>-3</sup>. The rms run length in each case is about 20, far in excess of the minimal acceptable value of 7 (Fig. 10). The density profiles roughly follow the Z-shaped pattern expected for cylindrical overturns, with the top half of the reordering regions consisting of heavier water and the bottom half of lighter water. The T–S relationship within these reordering regions is tight, the ξ values, 0.03 and 0.05, being very low.

## 6. Discussion

The EUBEX case contains many reordering regions that might be taken as overturning signatures if no criteria were applied other than the mere existence of density inversions. However, none of these passed our run-length and water-mass tests (Table 2). The run-length test rejected many reordering regions appearing in areas of low stratification, including a dramatically thick 400-m reordering region, which we know cannot have resulted from a single overturn (based on energy constraints). The remaining reordering regions are mostly located at interleaving locations. The water-mass criterion rejects all of these, and visual inspection of the  $T$ - $S$  diagrams confirms the presence of looping characteristic of time-constant mismatches. Thus, as expected from our initial estimates of resolution constraints, inference of mixing from CTD signals is not possible in the EUBEX case.

The SLE case, by contrast, appears to have large enough mixing, high enough stratification and fine enough depth-density resolution to allow inference of mixing from the reordering technique. Again, this is in line with our preliminary resolution estimates.

However, it should be emphasized that many SLE reordering regions failed our tests, suggesting that caution must be exercised even in resolvable regimes. Figures 14 and 15 illustrate this.

Figure 14 is in the same format as Fig. 7 except that the Thorpe displacements are only shown for accepted reordering regions. Comparison of the figures illustrates clearly that many small reordering regions have been eliminated, particularly in the regions of large Richardson number, where mixing is not expected to occur. This improved correspondence between regions of low  $Ri$  values and our revised estimate of mixing locations is encouraging.

Histograms of a surrogate for mixing intensity further support the suggestion that our procedure has successfully rejected spurious inversions. Figure 15a shows the SLE distribution of APEF  $N$ , which is proportional to  $\epsilon$  according to (2). The histogram for all the reordering regions is less symmetric than the histogram of those that pass through our noise-rejection filters, which is in line with the expected lognormal distribution of mixing signals. The prefiltered histogram is strongly skewed toward small values of APEF  $N$ , or small mixing values. Since  $APEF = L_T^2 N^2 / 2$  for a cylindrical overturn, and since the  $N$  in the reordering regions was fairly constant (about  $0.015 \text{ s}^{-1}$ , with an interquartile range of 50%), we interpret the histogram as being skewed to small values of Thorpe scale  $L_T$ . To investigate this further, we assumed  $L_T \approx L_r \delta z$ , where  $L_r$  is the run length distributed according to the noise PDF (9). Converting the PDF to a histogram by using a scale factor to match the observed number of reordering regions, we derive the noise histogram shown in Fig. 15b. This curve is in good qualitative

TABLE 2. Results of filtering reordering regions.

Number of reordering regions	SLE	EUBEX
In total	1640	110
With $n > 4$ points	560	27
As above plus passing run-length test	84	3
As above plus passing water-mass test	59	0

agreement with the histogram of discarded reordering regions, also shown in the figure. Both histograms are strongly skewed to low mixing rates, with a cutoff value at APEF  $N \sim 10^{-10} - 10^{-9} \text{ m}^2 \text{ s}^{-3}$ . The similarity of the noise histogram and the rejected histogram, together with the marked difference between each and the filtered histogram in Fig. 15, further supports our contention that our filtering process rejects spurious inversions.

It is worth noting that the log-mean value of prefiltered and filtered APEF  $N$  histograms differ by over an order of magnitude, so that  $\epsilon$  will vary by the same amount and so will the vertical eddy diffusivity  $K_v$ . Thus, processing the complete set of reordering regions, even in a nominally resolvable dataset like SLE, could yield inaccurate results.

## 7. Summary and conclusions

We have outlined a procedure that indicates when mixing conditions can be inferred reliably using a reordering technique.

The first step is to examine the preliminary resolution requirements on overturn thickness and dissipation rate, which are easily calculated [e.g., Table 1; Eqs. (4), (6), (7), and (8)]. In cases where these resolution limits exceed expected signal amplitudes, there may be little point in going through the reordering analysis. In cases that appear to be resolvable, we suggest two further tests to reject reordering regions that cannot be distinguished from noise.

The second step is to calculate the run lengths of Thorpe fluctuations in sample representative density profiles. By comparing the PDF of this quantity to the PDF for density noise added to a linear, gravitationally stable profile, we derive a threshold run length (e.g., Fig. 3). Reordering regions with rms run lengths below this limit are discarded, since they are indistinguishable from the result of random noise in regions of low stratification. This selection procedure is potentially very useful, because regions of low  $N^2$  are often regions of low Richardson number, where one might expect mixing to occur. Thus, we hope that the run-length criterion will reject spurious mixing signals that might otherwise be regarded with little suspicion.

The third step in our analysis eliminates remaining reordering regions caused by systematic, rather than random, CTD errors. In particular, we hope to discard inversions caused by  $T$ - $S$  ‘‘looping’’ associated with

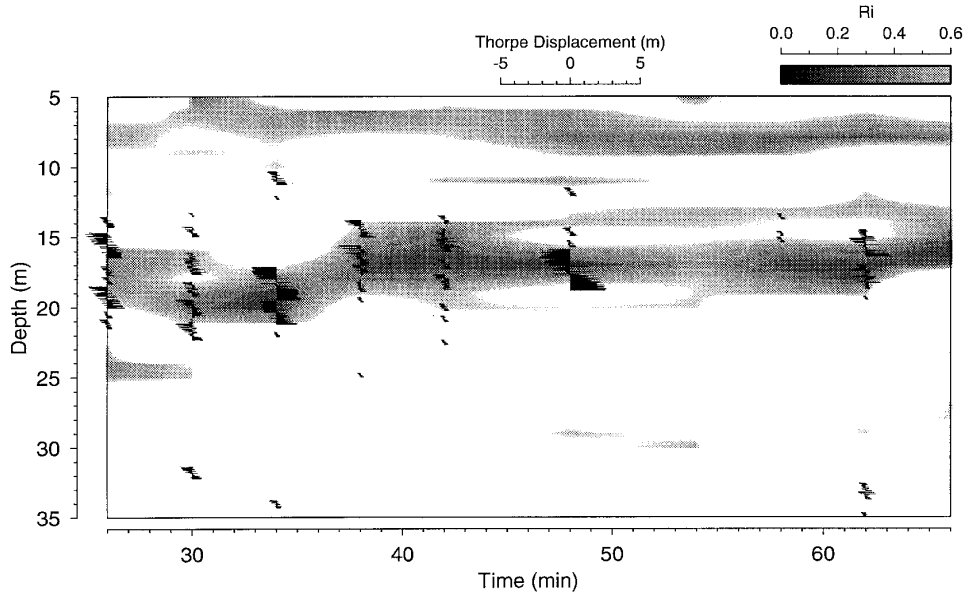


FIG. 14. As in Fig. 7 but for reordering regions that pass our quality tests. Note the improved match to areas of low Richardson number.

time-constant mismatches in sensors. Our method examines the  $T$  and  $S$  contributions to  $\rho$  independently. We require that variation about a linear  $T-S$  model be small, in density terms, compared to the overhanging density anomaly of the inversion itself. Thus, we hope to accommodate situations of arbitrary density ratio, allowing application in interleaving regions.

Our test procedure was calibrated with examples representing opposite ends of the application spectrum: 1) a highly stratified, vigorously mixed, coastal environment and 2) a weakly stratified, weakly mixed deep-ocean environment. Our test cases also span the range of CTD resolution, the coastal case having fine resolution and the deep-sea case having coarse resolution. Our preliminary comparison of resolution limits and expected mixing signals suggested that the reordering

technique would fail in the deep-sea case and work in the coastal case. This prediction was correct. The deep-sea case had no reordering regions that our tests could distinguish from noise or systematic  $T-C$  errors. In contrast, the coastal case showed many reordering regions that passed our tests. Encouragingly, these accepted reordering regions are predominantly found in regions of low Richardson number where mixing is expected. This point is made clearly in Figs. 7 and 14. Furthermore, the histogram of APEF  $N$ , a surrogate for dissipation rate, was roughly lognormally distributed but *only* after spurious reordering regions had been rejected (Fig. 15). These results suggest that our procedure is effective in rejecting spurious inversions in CTD profiles and that reordering regions that pass our tests are likely to represent actual mixing events.

*Acknowledgments.* We acknowledge financial support from NSERC. We thank E. L. Lewis and R. G. Perkin for providing us with the EUBEX data. PSG completed part of this work while at the Department of Atmospheric and Oceanic Sciences, McGill University, and wishes to thank R. G. Ingram for providing time to work on this paper.

REFERENCES

Caulfield, C. P., and W. R. Peltier, 1994: Three dimensionalization of the stratified mixing layer. *Phy. Fluids*, **6**, 3803–3805.  
 Crawford, W. R., 1986: A comparison of length scales and decay times of turbulence in stably stratified flows. *J. Phys. Oceanogr.*, **16**, 1847–1854.  
 Cullen, J. J., E. Stewart, E. Renger, R. W. Eppley, and C. D. Winant, 1983: Vertical motion of the thermocline, nitracline and chlorophyll maximum layers in relation to currents on the Southern California Shelf. *J. Mar. Res.*, **41**, 239–262.

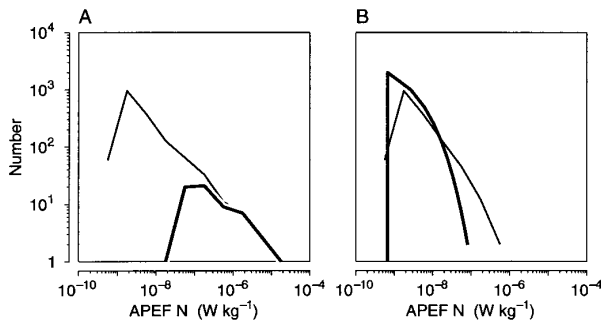


FIG. 15. (a) Histograms of surrogate for dissipation rate for all reordering regions in SLE (thin line) and for just those that pass our noise-rejection tests (thick line). (b) Histogram for noise (thick line) compared to histogram of rejected reordering regions (thin line).

- Dillon, T. M., 1982: Vertical overturns: A comparison of Thorpe and Ozmidov length scales. *J. Geophys. Res.*, **87**, 9601–9613.
- , 1984: The energetics of overturning structures: Implications for the theory of fossil turbulence. *J. Phys. Oceanogr.*, **14**, 541–549.
- , and M. M. Park, 1987: The available potential energy of overturns as an indicator of mixing in the seasonal thermocline. *J. Geophys. Res.*, **92**, 5345–5353.
- Hebert, D., J. N. Moum, C. A. Paulson, and D. R. Caldwell, 1992: Turbulence and internal waves at the equator. Part II: Details of a single event. *J. Phys. Oceanogr.*, **22**, 1346–1256.
- Horne, E. P. W., and J. M. Toole, 1980: Sensor response mismatches and lag correction techniques for temperature–salinity profilers. *J. Phys. Oceanogr.*, **10**, 1122–1130.
- Koch, S. E., M. DesJardins, and P. J. Kocin, 1983: An interactive Barnes objective map analysis scheme for use with satellite and conventional data. *J. Climate Appl. Meteor.*, **22**, 1487–1503.
- Larson, R. J., and M. L. Marx, 1986: *An Introduction to Mathematical Statistics and its Application*. 2d ed. Prentice-Hall, 630 pp.
- Levitus, S., 1982: Climatological atlas of the World Ocean. NOAA Prof. Paper 13, 173 pp.
- Lewis, E. L., and R. G. Perkin, 1983: Supercooling and energy exchange near the arctic ocean surface. *J. Geophys. Res.*, **88**, 7681–7685.
- Lueck, R. G., 1990: Thermal inertia of conductivity cells: Theory. *J. Atmos. Oceanic Technol.*, **7**, 741–755.
- , and J. J. Picklo, 1990: Thermal inertia of conductivity cells: Observations with a Sea-Bird cell. *J. Atmos. Oceanic Technol.*, **7**, 756–768.
- Mack, S. A., 1989: Towed-chain measurements of ocean microstructure. *J. Phys. Oceanogr.*, **19**, 1108–1129.
- , and H. C. Schoeberlein, 1993: Discriminating salt-fingering form turbulence-induced microstructure: Analysis of towed temperature–conductivity chain data. *J. Phys. Oceanogr.*, **23**, 2073–2106.
- MacKenzie, B. R., and W. C. Leggett, 1991: Quantifying the contribution of small-scale turbulence to the encounter rates between larval fish and their zooplankton prey: Effects of wind and tide. *Mar. Ecol. Prog. Ser.*, **73**, 149–160.
- McGowan, J. A., and T. L. Hayward, 1978: Mixing and oceanic productivity. *Deep-Sea Res.*, **25**, 771–793.
- Morison, J. H., R. Anderson, N. Larson, E. D'Asaro, and T. Boyd, 1994: The correction for thermal-lag effects in Sea-Bird CTD data. *J. Atmos. Oceanic Technol.*, **11**, 1151–1164.
- Moum, J. N., 1990: The quest for  $K\rho$ —Preliminary results from direct measurements of turbulent fluxes in the ocean. *J. Phys. Oceanogr.*, **20**, 1980–1984.
- Muelbert, Z. H., M. L. Lewis, and D. E. Kelley, 1994: The importance of small-scale turbulence in the feeding of herring larvae. *J. Plankton Res.*, **16**, 927–944.
- Ozmidov, R. V., 1965: On the turbulent exchange in a stably stratified ocean. *Izv. Acad. Sci., USSR, Atmos. Oceanic Phys.*, **1**, 853–860.
- Padman, L., and T. M. Dillon, 1991: Turbulent mixing near the Yermak plateau during the coordinated Eastern Arctic experiment. *J. Geophys. Res.*, **96**, 4769–4782.
- Perkin, R. G., and E. L. Lewis, 1982: Design of CTD observational programmes in relation to sensor time constants and sampling frequencies. Canadian Tech. Rep. of Hydrography and Ocean Sciences 7, Institute of Ocean Sciences, 47 pp.
- , and ———, 1984: Mixing in the West Spitsbergen current. *J. Phys. Oceanogr.*, **14**, 1315–1325.
- Peters, H., M. C. Gregg, and J. M. Toole, 1988: On the parameterization of equatorial turbulence. *J. Geophys. Res.*, **93**, 1199–1218.
- , ———, and T. B. Sanford, 1995: Detail and scaling of turbulent overturns in the Pacific Equatorial Undercurrent. *J. Geophys. Res.*, **100**, 18 349–18 368.
- Rothschild, B. J., and T. R. Osborn, 1988: Small-scale turbulence and plankton contact rates. *J. Plankton Res.*, **10**, 465–474.
- Seim, H. E., and M. C. Gregg, 1994: Detailed observations of a naturally occurring shear instability. *J. Geophys. Res.*, **99**, 10 049–10 073.
- Sverdrup, H. U., 1955: The place of physical oceanography in oceanographic research. *J. Mar. Res.*, **14**, 287–294.
- Thorpe, S. A., 1977: Turbulence and mixing in a Scottish loch. *Philos. Trans. Roy. Soc. London, Ser. A*, **286**, 125–181.
- , 1984: The transition from Kelvin–Helmholtz instability to turbulence. *Internal Gravity Waves and Small-Scale Turbulence*, P. Muller and R. Pujale, Eds., Hawaii Institute of Geophysics, 65–76.
- , 1985: Laboratory observations of secondary structures in Kelvin–Helmholtz billows and consequences for ocean mixing. *Geophys. Astrophys. Fluid Dyn.*, **34**, 175–199.
- , A. J. Hall, C. Taylor, and J. Allen, 1977: Billows in loch ness. *Deep-Sea Res.*, **24**, 371–379.
- Topham, D. R., and R. G. Perkin, 1988: CTD sensor characteristics and their matching for salinity calculations. *IEEE J. Oceanic Eng.*, **13**, 107–117.
- Washburn, L., 1987: Two-dimensional observations of temperature microstructure in a coastal region. *J. Geophys. Res.*, **92**, 10 787–10 798.
- Woods, J. D., 1968: Wave-induced shear instability in the summer thermocline. *J. Fluid Mech.*, 791–800.
- Yamazaki, H., and T. Osborn, 1993: Direct estimation of heat flux in a seasonal thermocline. *J. Phys. Oceanogr.*, **23**, 503–516.